Journal of Molecular Graphics and Modelling 34 (2012) 46–56

Contents lists available at SciVerse ScienceDirect

Journal of Molecular Graphics and Modelling

journal homepage: www.elsevier.com/locate/JMGM

Theoretical study on the electronic structure and optical properties of carbazole-π-dimesitylborane as bipolar fluorophores for nondoped blue OLEDs

Y. Zhang, L.L. Zhang, R.S. Wang, X.M. Pan*

Faculty of Chemistry, Institute of Functional Material Chemistry, Northeast Normal University, Changchun 130024, People's Republic of China

ARTICLE INFO

Article history:
Received 27 June 2011
Received in revised form
21 December 2011
Accepted 22 December 2011
Available online 2 January 2012

Keywords:
Bipolar fluorophores
DFT
TDDFT
PCM
ab initio calculations

ABSTRACT

Molecules with D-π-A structures are drawing increased attention for applications in organic electronic devices due to their distinct optoelectronic properties. A study of a new series of bipolar fluorophores that have been chemically modified for use as highly efficient nondoped blue organic light-emitting diodes (OLEDs) has been carried out based on existing molecular structures and a literature survey. The aim of this study is to provide a profound interpretation of the optical and electronic properties and the structure–property relationships of a series of new bipolar fluorophores. The study also aims to predict the photophysical and optoelectronic properties of the new fluorophores. The density functional theory (DFT) has been confirmed as reliable, especially in predicting the properties of unknown products. The geometry and the electronic structure of these molecules in the ground state were studied with DFT and *ab initio* HF, whereas the lowest singlet excited-state geometries were optimized by *ab initio* singlet configuration interaction (CIS). The absorption and emission spectra, both in the gas phase and in THF, and the lowest singlet excited energies were calculated by employing the time-dependent density functional theory (TDDFT) and the polarizable continuum model (PCM). To precisely predict the charge-transporting and charge-confining properties of the new fluorophores, three-layered devices have been simulated. The results show that the molecular geometries, HOMOs, LUMOs, energy gaps, ionization potentials (IP), electron affinities (EA), radiative lifetimes (τ), absorption and emission spectra are all tuned by chemical modifications with different π-conjugated bridges. The results also show that these molecular materials could be used as bipolar light-emitting materials for blue and deep-blue OLEDs.

1. Introduction

Recently, organic light-emitting diodes (OLEDs) have exhibited great potential for applications such as flat panel displays and solid-state lighting devices [1–4] and are attracting the attention of many researchers. Several green and red organic light-emitting materials have been developed for full-color displays, but highly efficient and stable blue light-emitting organic materials are still rare [5–7]. It is difficult to design and synthesize blue light-emitting materials of high efficiency, color purity, and long operational time due to their wide energy gap [8–10]. In other words, balancing the process of the injection of holes from the anode with electrons from the cathode in blue light-emitting OLEDs is difficult. The fact that a dopant-host system can significantly enhance the performance of a device such as its electroluminescence (EL), quantum yield, emissive color, and operational lifetime is well known [11]. However, EL properties, such as color purity, are extremely sensitive to the dopant concentration [12–14]. Doped OLEDs are more difficult to adapt to practical applications than their nondoped counterparts [15]. Therefore, the ability to design high-performance blue light-emitting materials for nondoped devices with high brightness and efficiency is essential and desired.

Light-emitting materials with bipolar structures would facilitate the formation of an exciton (*via* stable cation and anion radicals) and improve charge balancing in OLEDs [16–18], both of which would improve the single-layer device performance of OLEDs and simplify their fabrication. Recently, molecular structures with electron donor and acceptor groups separated by a π-conjugated core (D-π-A) have found many applications in fluorescence technologies, chemoluminescence, and photovoltaics [19–22]. Lin et al. have designed and synthesized a series of carbazole-π-dimesitylborane bipolar fluorophores as efficient light-emitting materials named czb, czphb, czthb, and czsb [14]. The photophysical properties and HOMO/LUMO energy levels of the four fluorophores have been determined and evaluated experimentally [14]. Two of these fluorophores, czthb and czphb in particular, exhibit good thermal stability, high color purity, and high external quantum efficiency (EQE) as multifunctional fluorophores. The influence of varying π-conjugations in light-emitting materials has been thoroughly studied not only in their configuration stabilization but also in

* Corresponding author. Tel.: +86 431 85099963; fax: +86 431 85099511.
E-mail address: panxm460@nenu.edu.cn (X.M. Pan).

1093-3263/$ – see front matter © 2012 Elsevier Inc. All rights reserved.
doi:10.1016/j.jmgm.2011.12.007

their electroluminescent properties. Furthermore, Ouyang et al. [23] investigated the micromechanism of the luminescent properties of czthb and czphb theoretically and calculated that the optical properties are in good agreement with the experimental data.

Based on the existing molecular framework and literature survey, slight chemical modifications have been carried out: four new molecules, czfub, czprb, czpyb, and czflb have emerged replacing various π-conjugated bridges to produce better multifunctional light-emitting materials for nondoped OLEDs. The incorporation of heteroatoms into the π conjugation is well known as an effective way to tune the optical properties of the materials. In addition, molecules with planar configurations are known to promote luminescent efficiency. Therefore, a π-conjugated bridge that can form a coplanar structure with a carbazole moiety is selected as the core. The calculated results demonstrate that czflb with a larger-sized core did not exhibit excellent EL properties, as originally predicted. In this study, the density functional theory (DFT), the singlet configuration interaction (CIS) methods, *ab initio* HF and time-dependent density functional theory (TDDFT) calculations have been carried out for the studied molecules. The highest occupied molecular orbitals (HOMOs), the lowest unoccupied orbitals (LUMOs), energy gaps, ionization potentials (IPs), electron affinities (EAs) and the radiative lifetimes (τ) have been thoroughly examined for the optical and electronic properties of these compounds. All of the calculated results would be expected to provide insight into the synthesis of new, highly efficient blue light-emitting materials.

2. Computational details

All calculations on the molecules described herein have been performed with the Gaussian 03 and Gaussian 09 program packages [24]. The calculated electronic density plots for the frontier molecular orbitals were prepared by GaussView 3.0 software. The B3LYP functional, involving the gradient correction to the exchange functional by Becke [25] and the correction functional by Lee et al. [26], has been used as the primary functional. For comparison, one of the M06 families of functionals for the prediction of electronic excitation energies, M06-2X [27–30], has been used to investigate the dependence of the functional. The 6-31G* basis set was employed for the singlet ground-state and first excited-state geometries. And for comparison, unrestricted formalism (UB3LYP) with the diffusion function 6-31+G* basis set was employed for the optimization of the ionic-state geometries. The primary bond lengths and bond angles obtained by both UB3LYP/6-31G* and UB3LYP/6-31+G* were found to be nearly identical for the cationic geometries. Therefore, the 6-31G* basis set is selected for all of the calculations. All excited-state geometries were optimized by the *ab initio* configuration interaction singles method (CIS). The electronic absorption and emission spectra in vacuum were carried out using the time-dependent density functional theory (TDDFT) method based on the optimized ground- and excited-state geometries, respectively. The polarizable continuum model (PCM) was adopted in the solvent (THF). And for comparison, the solvation model of density (SMD) has also been used to predict the solvation effect. The solvation effects were only used in the prediction of the absorption and emmision spectra. The various properties of these compounds such as the HOMO and LUMO energies, the energy gap (Eg), the IPs and the EAs were derived from the computed results.

3. Results and discussion

3.1. Significance of the study

To confirm the validity of the DFT method, we performed a literature survey and DFT calculations. As shown in Table S2, the calculated absorption data (408.3 nm and 386.9 nm) for czthb and czphb in THF are in good agreement with the experimental data (390.0 nm and 354.0 nm). The emission data (450.1 nm and 425.3 nm) for czthb and czphb are also comparable to their corresponding experimental values (455.0 nm and 436.0 nm) [14]. Ouyang et al. obtained the same conclusion using the same computational process. The HOMO, LUMO energy levels obtained by Ouyang [23] under the same calculating level are all in good agreement with our calculated results (Tabe S1). Therefore, this theoretical method can be regarded as a reasonable tool for the prediction of the properties of new fluorophores.

Carbazole-based compounds have received a great deal of attention for the following reasons: (1) with a good aromatic structure, they can provide a highly efficient fluorescence with better chemical and environmental stability; (2) their nitrogen atom can easily be substituted with a variety of functional groups to tune the optical and electrical properties; and (3) they can exhibit the bifunctional properties of light-emission and hole-transportation (HT) [31]. In addition, boron derivatives have been demonstrated that they can serve as electron-transporting (ET) materials due to the electron-deficient characteristic of the boron center [18].

On the basis of the existing molecular framework and the literature survey, a series of new molecules, czfub, czprb, and czpyb (Fig. 1), have emerged *via* chemical modification. Incorporating heteroatoms into the π-conjugation of these organic materials is an effective way to tune the electronic structure of the molecules. The nonplanar configuration of dimesitylborane can efficiently prevent the close packing of the molecules in the solid state and thus increase the glass transition temperature for the formation of smooth films. The coplanar feature of the carbazole moiety and the core molecule can promote the luminescent efficiency. In their experimental reports, researchers devoted their attention to extending the linear length of the alkyl chain in the π conjugation. Although linear extension of the π conjugations is known to promote the luminescent strength, it also lowers the molecular rigidity and causes a large bathochromic shift. These results are primarily due to the less-rigid configuration of a molecule with more single bonds leading to nonradioactive dissipation that is sensitive to blue-light materials such as czsb, as shown in the experimental report [14]. In the present research, we changed the π-conjugated electronic density, but not the π-conjugation structure size. Furthermore, to allow for comparison and to confirm the above supposition, another fluorene-based material with a larger-sized core, czflb, has emerged in the series of promising blue-light materials with rigid plane configurations.

3.2. Geometry optimization

3.2.1. The neutral-ground-state and charged-state geometries

Sketch maps for the four studied compounds are depicted in Fig. 1, and the structural parameters of czfub, czprb, czpyb, and czflb in the isolated gas phase have been computed at the B3LYP/6-31G* level, and their optimized structures are plotted in Fig. 2. The nitrogen and boron cores and their relevant geometry parameters in the neutral, cationic and anionic states have received special attention and have been obtained by B3LYP/6-31G*, as shown in Table 1. The calculated results have revealed similar trends in the variations of bond lengths and bond angles in both neutral and charged states for the title compounds.

Fig. 1 clearly shows that the title compounds have the same framework on both sides of the molecule, but different π-conjugated groups in the center. The carbazole segment exhibits a highly planar configuration due to the dihedral angle between the two phenyl rings in the carbazole segment that is fixed by a ring-bridged nitrogen atom with a single electron pair, which tends to keep its aromatic structure. Additionally, the dimesitylborane segment exhibits a highly nonplanar configuration. As shown in

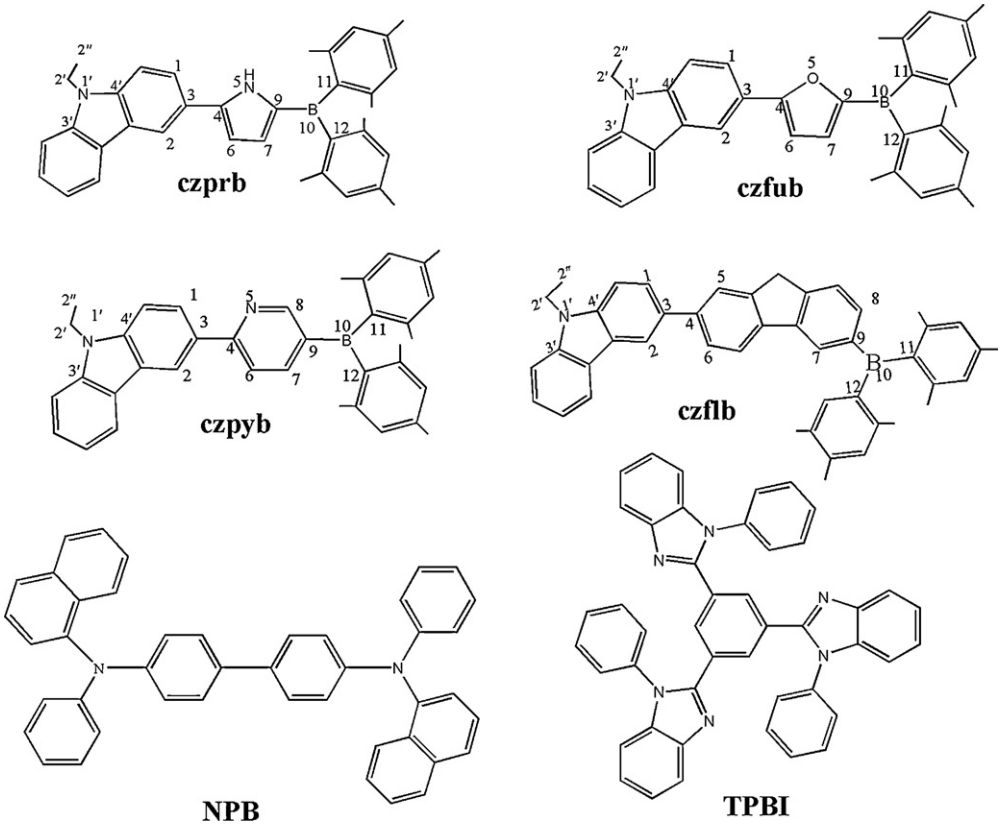

Fig. 1. Sketch map of the studied structures.

Table 1, the angles around both the N and B atoms in the title compounds for θ(2′,1′,4′), θ(3′,1′,2′), θ(3′,1′,4′), θ(9,10,11), θ(9,10,12), and θ(11,10,12) are very close to each other, both in the neutral and charged states. The sums of these angles around both the N and B atoms are very close to 360°, indicating that nitrogen and boron with three carbon atoms exhibit highly planar configurations. This conclusion coincides with the dihedral angles ϕ(9,10,11,12) (179.7°, −178.9°, 179.8°, and −179.9°). However, these two segments are not coplanar with each other except in the cases of czfub and czpyb. As is well known, molecules with highly rigid configurations lessen the probability of internal conversion and correspondingly increase the fluorescent quantum efficiency; therefore, czfub and czpyb could exhibit higher quantum efficiency than other molecules.

As shown in Table 1, in the neutral geometry, the bond lengths r(9,10) of czfub, czprb, czpyb, and czflb are 1.527 Å, 1.532 Å, 1.565 Å, and 1.569 Å, respectively, indicating that the inter-ring bridge bond strength gradually decreases. The significantly strengthened B–C bond in czprb is primarily due to the electron-rich nature of the five-membered heterocyclic rings: the greater the electron density, the stronger the bridge bond. The bridge bonds between the carbazole segments and the π-conjugated groups for czpyb and czflb, bond lengths r(3,4), are noticeably longer than those of czprb and czfub. This observation can also be ascribed to the electron-rich nature of π-conjugated groups. The absolute values of the dihedral angles, ϕ(1,3,4,6), of czfub, czprb, czpyb, and czflb are 155.5°, 178.6°, 164.4°, and 142.7°, respectively, indicating that only the carbazole and furan moieties of czfub are nearly coplanar. The absolute values

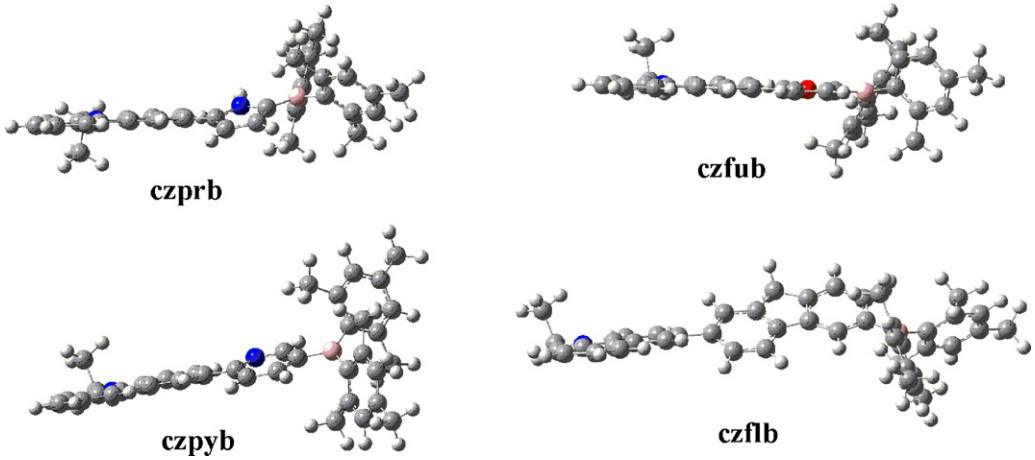

Fig. 2. The stereograph of optimized title compounds by DFT//B3LYP/6-31G*.

Table 1
Selected important bond length (angstroms), bond angles (degrees), and dihedral angles (degrees) of title compounds obtained by B3LYP/6-31G* calculations.

	czprb			czfub			czpyb			czflb		
	Neutral	Cationic	Anionic	Neutral	Cationic	Anionic	Neutral	Cationic	Anionic	Neutral	Cationic	Anionic
r(1, 3)	1.416	1.430	1.428	1.416	1.431	1.428	1.416	1.429	1.424	1.415	1.430	1.416
r(2, 3)	1.403	1.424	1.418	1.403	1.423	1.415	1.403	1.421	1.410	1.402	1.422	1.402
r(3,4)	1.464	1.428	1.443	1.457	1.423	1.437	1.482	1.464	1.469	1.485	1.455	1.484
r(4, 5)	1.363	1.376	1.388	1.353	1.361	1.376	1.351	1.357	1.366	1.409	1.424	1.411
r(4, 6)	1.404	1.430	1.405	1.384	1.405	1.391	1.409	1.413	1.416	1.409	1.427	1.408
r(7, 9)	1.406	1.424	1.418	1.386	1.401	1.407	1.410	1.407	1.431	1.412	1.401	1.427
r(9,10)	1.527	1.572	1.532	1.532	1.567	1.516	1.565	1.581	1.533	1.569	1.586	1.551
θ(2′,1′,4′)	125.7	126.2	125.3	125.7	126.1	125.2	125.7	126.0	125.3	125.7	126.0	125.5
θ(3′,1′,2′)	125.6	124.7	126.0	125.6	124.6	125.9	125.5	124.7	125.9	125.6	124.8	125.8
θ(3′,1′,4′)	108.5	109.0	108.5	108.6	109.2	108.5	108.6	109.3	108.5	108.5	109.1	108.5
θ(9,10,11)	117.6	115.6	118.9	119.8	118.5	121.2	118.8	118.9	120.4	119.0	118.7	120.0
θ(11,10,12)	123.6	126.0	122.1	123.9	125.6	121.6	118.4	117.8	119.6	119.0	117.6	119.8
θ(9,10,12)	118.8	118.4	119.1	116.3	115.8	117.2	122.8	123.3	119.9	122.1	123.7	120.2
ϕ(1,3,4,6)	−155.5	175.1	−166.6	178.6	179.2	−179.9	−164.4	−173.5	178.8	−142.7	156.0	143.4
ϕ(5,9,10,12)	170.3	164.2	165.2	169.0	162.4	169.8						
ϕ(8,9,10,12)		−156.0	−151.0	−165.1	154.5	151.0	161.2					
Φ(9,10,11,12)	179.7	179.6	179.7	178.9	−178.8	−178.5	179.8	179.8	179.6	−179.9	179.8	−179.8
ϕ(2″,2′,1′,3′)	−87.2	−84.45	−88.85	87.3	84.45	88.23	86.0	84.85	88.36	80.00	85.46	87.59
dipole moment	4.47			3.77			2.16			3.18		

of the dihedral angles, ϕ(5,9,10,12) or ϕ(8,9,10,12), of czfub, czprb, czpyb, and czflb are 170.3°, 169.0°, 156.0°, and 154.5°, respectively, indicating that the incorporation of a six-membered heterocyclic ring and an even larger π-conjugated fluorene group into the dipole-featured molecules create much greater steric hindrance. As previously mentioned, the carbazole group and the boron atom surrounded by three carbon atoms have planar configurations; therefore, it is reasonable to select these two segments as the reference plane. From the values of the dihedral angles ϕ(2″,2′,1′,3′), the values of czprb are found to be negative in both the neutral and charged states; the location of the ethyl group in czprb is opposite to its location in other compounds. This condition may be attributed to the remarkable interaction between the hydrogen atom of the pyrrole group and the other five hydrogen atoms of the ethyl group.

It can be easily observed from the HOMO and LUMO characters in Fig. 3 that an antibonding character exists between the bridged atoms of the inter-ring, and a bonding character exists between the carbon and carbon atoms of intra-ring in the HOMO. The opposite case is true for the LUMO. Therefore, removing an electron from the HOMO will lead to the shortening of the inter-ring bond length. In contrast, the acceptance of an electron will lengthen the bond length in these regions. In summary, the structures of the charged states tend toward more planar and rigid configurations.

3.2.2. The lowest singlet excited-state (S_1) geometry

The first singlet excited-state geometries of the title compounds derived using CIS/6-31G* and the corresponding ground state structures obtained with HF/6-31G* are shown in Table 2. As shown, some of the bond lengths are extended, but some are shortened. The differences between these in the ground state (S_0) and in the first singlet excited state (S_1) can be predicted from the location of the nodes of the frontier molecular orbitals because the first singlet excited state corresponds to an excitation from the HOMO to the LUMO in each of the considered compounds. The variation in the bond lengths can be explored by investigating the composition features of the HOMO and LUMO contours. Table 2 and Fig. 3 show that the LUMOs have nodes across *r*(1,3), *r*(2,3), *r*(4,5), *r*(4,6), and *r*(7,9) in the title compounds, but the HOMOs also bond in the abovementioned regions, allowing for the prediction that the bond lengths in these regions in the first singlet excited state will be lengthened. In fact, as shown in Table 2, these bonds are indeed lengthened in the lowest singlet excited state, and the bond lengths contract when changing from antibonding to bonding. As shown in Fig. 3, the HOMO contours have nodes across the bonds *r*(3,4) in each of the title compounds, while the LUMO contours also bond in these regions. Therefore, the data corroborates the above prediction. According to their absolute value, the dihedral angles ϕ(1,3,4,6) of czfub, czprb, czpyb, and czflb, both in the ground state and in the first singlet excited state, increase from 145.1°, 176.3°, 155.8°, and 134.5° to 174.7°, 179.4°, 180.0°, and 169.2°, respectively. Obviously, the lowest singlet excited-state structure exhibits a strong coplanar trend in these compounds, which can be attributed to strongly electronic delocalization in the first singlet excited-state structure. Furthermore, the primary characteristics and changing trends in bond lengths, bond angles and dihedral angles calculated in both the B3LYP/6-31G* and HF/6-31G* levels are quite close to each other. The dipole moments found in Tables 1 and 2 demonstrate that czprb with a pyrrol π-conjugated bridge has better electron push-pull ability both in the ground and first-singlet-excited states and that the push–pull ability in the excited state is stronger than it is in the ground state. One can further predict that the electronic properties of czprb will be easily influenced by their environment.

3.3. Frontier molecular orbitals

The HOMOs and LUMOs for the title compounds have been investigated at the B3LYP/6-31G* level, and the electron contours of the frontier molecular orbitals and the orbital energy levels have been plotted in Fig. 3 and Table 3. Confirmation of the energy levels of the HOMO and LUMO of these molecules would prove useful. The ordering of the occupied and virtual orbitals provides a reasonable qualitative indication of the excitation properties [32] and of their ability for electron- or hole-transport. Because the first dipole-allowed electronic transition is the strongest electronic transition with the largest oscillator strength, it usually corresponds to the promotion of an electron from HOMO to LUMO. More importantly, the differences in the optical and chemical properties of compounds usually rely on changes in the electronic structures and the frontier molecular orbitals of the compounds in the ground state.

As shown in Fig. 3, the frontier molecular orbitals of the title compounds are spreading over their entire π-conjugated backbones, although the largest contributions come from different regions of the molecular structure. The electron density contributions of each moiety have been plotted in Fig. 3. The first three molecules exhibit a similar electron density contribution, so we list their average values. The HOMOs possess antibonding character between their subunits, indicating that nonplanar character could be observed in these molecules in their ground states. In

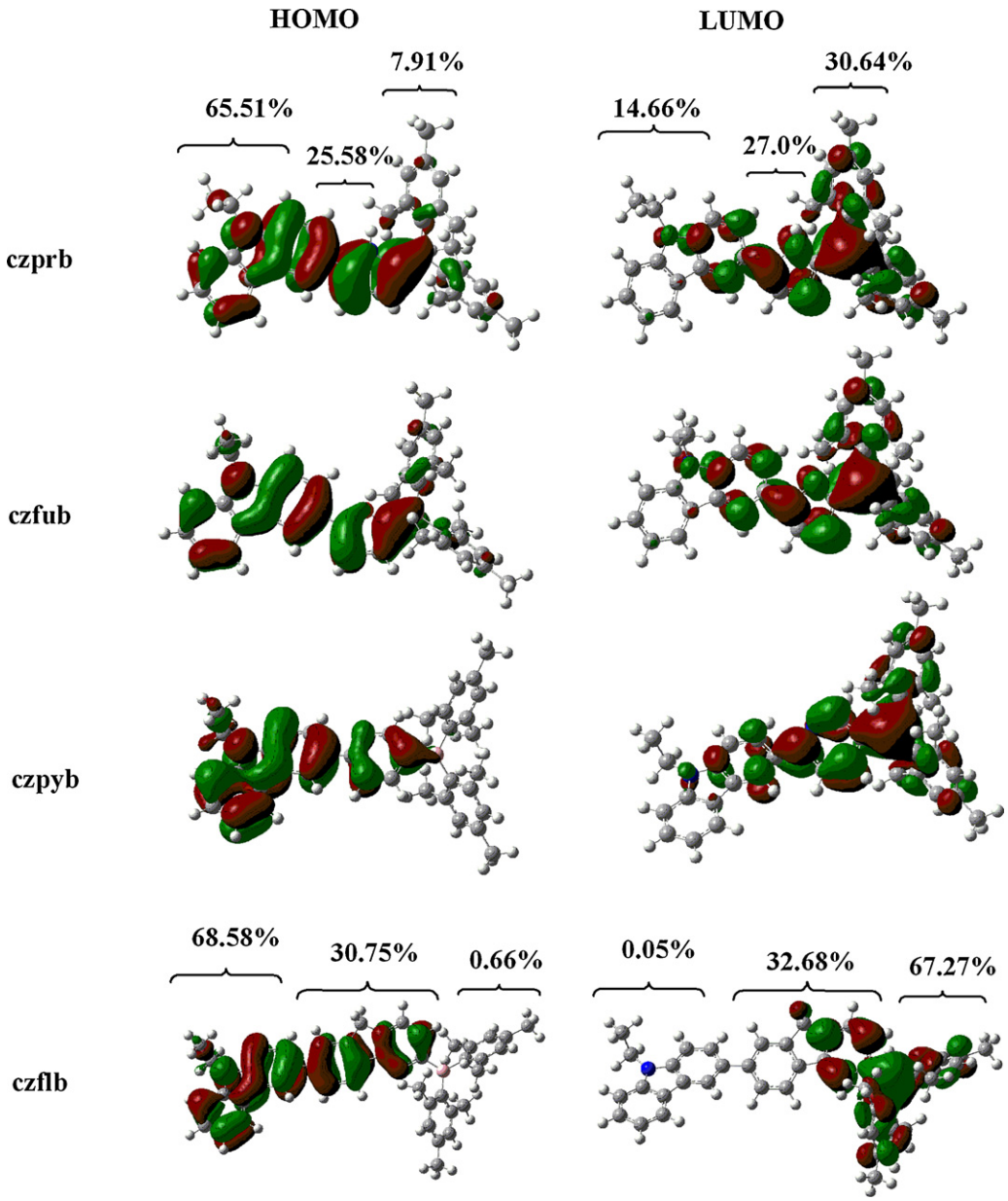

Fig. 3. Electronic density contours of the frontier orbitals for the title compounds, and the contributions of the electron density of each moiety.

contrast, the LUMOs of each of the molecules generally show bonding character between the subunits, implying that the lowest singlet excited state, which primarily involves the promotion of an electron from the HOMO to the LUMO, would be more planar. The electron density data shows that the electronic cloud distribution is strongly confined to the carbazole moiety in the HOMO due to the largest contribution of the planar skeleton of carbazole, whereas for the LUMO, the electron clouds are largely transferred to the dimesitylborane section. These observations imply that the ethyl carbazole moiety serves in an electron-donating role, and its electron density is strengthened when the core molecule is altered from a five-membered aromatic ring to a six-membered aromatic ring, or even to fluorene. However, after replacing the aromatic ring with the larger fluorene, the HOMO is primarily localized on the carbazole and fluorene with a dominating electron density contribution, while the nonplanar dimesitylborane has the greatest contribution to the LUMO, indicating that fluorene has a strong electron-donating ability with an effectively improved HOMO level and can greatly facilitate the intramolecular charge transfer.

In the experimental method, the HOMO energy levels of the title compounds were determined by low-energy photo-electron spectrometry (Riken-keiki AC-2). Concurrently, the LUMO energy levels were estimated by subtracting the energy gap (E_{gap}, estimated from the absorption on-set energy) from the HOMO energy levels in the solid state [14]. The HOMO and LUMO energies were calculated by DFT in this study. The HOMO and LUMO energy levels of the title compounds are listed in Table 3. HT materials with higher HOMO energy levels lose their electron, or accept a hole, more easily, and ET materials with lower LUMO energy levels accept an electron more easily. Electron-rich groups elevate the HOMO energy level, and electron-deficient groups lower the LUMO energy level.

Fig. S1 shows that, by replacing the sulfur in czthb with nitrogen and oxygen atoms, the resulting fluorophores (czprb and czfub) exhibit both increased HOMOs and LUMOs due to the stronger electron-donation ability of the N and O atoms. While replacing

Table 2
Selected important bond length (Angstroms), bond angles (Degrees), and dihedral angles (Degrees) of title compounds in ground state and the first excited state obtained by HF/6-31G* and CIS/6-31G* calculations.

	czprb		czfub		czpyb		czflb	
	hf	cis	hf	cis	hf	cis	hf	cis
r(1,3)	1.403	1.434	1.403	1.435	1.405	1.445	1.403	1.438
r(2,3)	1.387	1.425	1.388	1.425	1.387	1.432	1.386	1.428
r(3,4)	1.474	1.407	1.467	1.399	1.487	1.415	1.491	1.425
r(4,5)	1.347	1.379	1.328	1.354	1.328	1.374	1.396	1.444
r(4,6)	1.379	1.427	1.359	1.412	1.396	1.431	1.396	1.446
r(7,9)	1.381	1.432	1.359	1.412	1.399	1.418	1.400	1.390
r(9,10)	1.540	1.545	1.547	1.538	1.574	1.551	1.581	1.583
θ(2′,1′,4′)	125.8	125.7	125.7	125.7	125.8	125.8	125.8	125.8
θ(3′,1′,2′)	125.8	125.4	125.7	125.3	125.7	125.2	125.8	125.6
θ(3′,1′,4′)	108.4	108.8	108.4	108.9	108.4	108.9	108.3	108.6
θ(9,10,11)	118.1	117.2	119.5	119.3	119.1	119.7	119.0	119.0
θ(9,10,12)	123.3	124.2	123.9	124.1	118.5	118.8	118.9	118.8
θ(11,10,12)	118.6	118.7	116.5	116.6	122.4	121.5	122.2	122.2
ϕ(1,3,4,6)	−145.1	−174.7	176.3	−179.4	−155.8	−180.0	134.5	169.2
ϕ(5,9,10,12)	170.0	166.6	169.8	169.6				
ϕ(8,9,10,12)					−157.7	−162.9	154.5	152.9
ϕ(9,10,11,12)	179.9	179.8	−178.6	−179.1	179.8	179.6	−179.9	−179.9
ϕ(2″,2′,1′,3′)	−87.54	−87.89	87.51	87.87	87.05	87.74	−87.84	−88.10
Dipole moment	3.77	4.16	2.70	3.97	1.21	3.18	2.40	2.90

Table 3
The values of HOMO and LUMO energies, HOMO–LUMO gaps calculated by DFT, and the lowest excitation energies calculated by TDDFT in eV for title compounds.

	czprb		czfub		czpyb		czflb	
E_{HOMO}	−5.04	(−6.25)[a]	−5.16	(−6.33)	−5.31	(−6.50)	−5.12	(−6.33)
E_{LUMO}	−1.30	(−0.44)	−1.60	(−0.81)	−1.80	(−1.04)	−1.55	(−0.76)
E_{H-L}	3.74	(5.81)	3.56	(5.52)	3.51	(5.46)	3.57	(5.57)
Eg(td)	3.35	(3.87)	3.17	(3.64)	3.14	(3.83)	4.32	(4.44)

[a] Values in parentheses are from the M06-2X method.

the phenyl group with pyridine causes the resulting fluorophore (czpyb) to exhibit both decreased HOMOs and LUMOs due to the low electron-donation ability of the electron-deficient pyridine. Following chemical modification, both the HOMO and LUMO of the title compounds decrease in the same orders: −5.04 eV (czprb) > −5.12 (czflb) > −5.16 eV (czfub) > −5.31 eV (czpyb) for the HOMOs, and −1.30 eV (czprb) > −1.55 (czflb) > −1.60 eV (czfub) > −1.80 eV (czpyb) for the LUMOs (Table 3). This decrease is identical to the order of the electron-rich character of the π-conjugated bridges. Generally, higher HOMO values lead to easier hole creation. N, N′-Diphenyl-N,N-bis-(1-naphthyl)-1,1-biphenyl-4,4-diamine (NPD) is a well-known HT material with a HOMO level of −5.5 eV [33]. The HOMO levels of the four compounds are all close to that of NPD, which shows their good HT ability. These compounds are also good ET materials due to the electron-deficient character of the empty P_π orbital of borane. The LUMO level of czpyb is very close to that of the widely used ET/hole blocking material, 2-(4-biphenylyl)-5-(4-tert-butylphenyl)-1,3,4-oxadiazole (PBD) (−2.4 eV) [29], indicating that czpyb could be a good trifunctional material. The other studied compounds possess both hole-transporting and light-emitting properties, and their HOMO and LUMO energy levels are close to those of czthb (Table S1).

3.4. Charge-transporting and charge-confining qualities

Efficient charge confinement of light-emitting materials is known to contribute to high EL efficiency. To precisely predict the charge-transporting and charge-confining quality of the new fluorophores, molecular simulations and quantum calculations have been carried out on the well-known HT material, 4,4′-bis[N-(1-naphthyl)-N-phenylamino] biphenyl (NPB), and the ET material, 1,3,5-tris(N-phenylbenzimidizol-2-yl) benzene (TPBI) (Fig. 1). However, there are some discrepancies between the calculated HOMO and LUMO levels (in THF) of NPB and TPBI and the experimental values (Fig. 4). Maybe, this is due to the deviation of theoretical simulation, especially in contrast with the experimental studies. As shown in Fig. 4, three-layered devices have been simulated using the concept based on the frontier molecular orbital energy level (in THF). All of the title molecules are capable of accepting holes and electrons simultaneously, and their charge confinements all correspond to the ideal product czthb (Fig. S1). This fact is evident in the large gaps (average 0.48 eV) between the LUMO energy levels of NPB and those of the title compounds, which retain electron carriers in the light-emitting layer. A fairly large gap

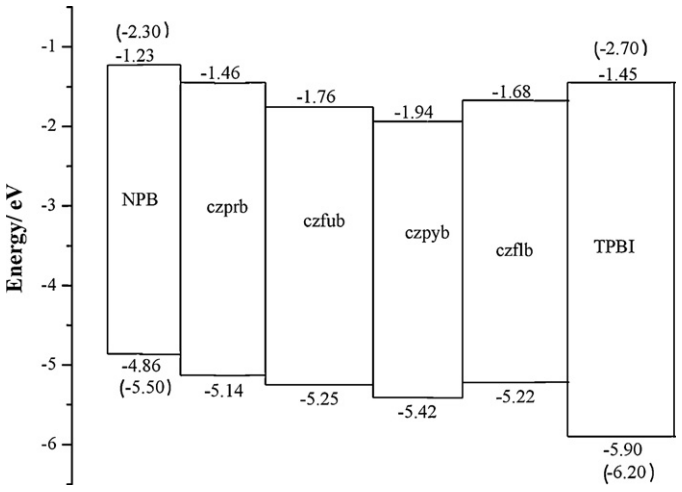

Fig. 4. The configuration of simulated three-layered OLEDs and theoretical energy (in THF) diagrams of the title compounds with the experimental values of NPB and TPBI in the brackets.

(average 0.64 eV) between the HOMO energy levels of the title compounds and TPBI retains hole carriers in the light-emitting layer as well. In addition, the LUMO energy differences between these compounds and TPBI are all small (average 0.26 eV), and czprb's LUMO level is rather close to that of TPBI. The HOMO energy differences between czprb or czflb and NPB are also relatively small. From the above mentioned properties, it can be observed that charge transporting and the excitons confinement in the light-emitting layer have shown ideal qualities for light-emitting materials.

3.5. HOMO/LUMO gaps and the lowest excitation energies

There are two theoretical approaches for obtaining the energy gaps described in this study. The first approach relies on the fact that the energy gaps for each of the compounds are estimated from the orbital energy differences between the HOMOs and LUMOs in the ground state [34]. The second approach utilizes the optical band gap, which is the lowest excitation energy from the ground-state to the first excited state calculated by TDDFT. The second method has been used to study systems of increasing complexity due to its relatively low computational cost and its consideration of electron correlation to extrapolate the energy gaps. In fact, the optical band gap is not the orbital energy difference between the HOMO and LUMO, but it is the energy difference between the S_0 state and the first dipole-allowed S_1 state. Only when the electronic transition to the first dipole-allowed S_1 state nearly corresponds to the promotion of an electron from the HOMO to the LUMO, can the optical band gap be approximately equal to the HOMO/LUMO gap. The HOMO/LUMO gaps (E_{H-L}) and the lowest singlet excited-state energies (Eg) are listed in Table 3. The E_{H-L} obtained by B3LYP/6-31G* are larger than the Eg values obtained by TDDFT//B3LYP/6-31G* calculations. This difference is due to the fact that the energy of a vertical electronic transition from an occupied molecular orbital (MO) to a vacant MO is predicted to be smaller than energy differences between the orbitals due to the inter-electronic interaction of a double-occupied MO upon single electron excitation. Although there are discrepancies between the E_{H-L} and Eg values, their trends remain the same. The ordering of the energy gaps for E_{H-L} and Eg is as follows: czprb > czflb > czfub > czpyb, indicating that the electron-donation ability of the core promotes the energy gaps. Except for czpyb, the E_{H-L} values of the remaining three compounds increased when compared with those of czthb and czphb (Table S1). Although the incorporation of a fluorene moiety was found to increase the size of the entire molecular electronic structure, it did not greatly contribute to the electronic density. The main reason for this observation is that electronic delocalization of entire molecular structure is limited, due to the more highly nonplanar geometry of czflb. Therefore, the HOMO, LUMO energy levels of czflb are very close to those of czfub. Blue light-emitting material with a large enough band gap (>3 eV) and a set of matching HOMO/LUMO energy levels is indispensable and would facilitate the performance of OLEDs [35]. As seen in Table 3, the Eg value for each of the compounds is larger than 3.0 eV, and each compound could qualify as a blue light-emitting material. Although the method for obtaining band gaps with orbital energy differences between the HOMO and LUMO is crude, it is still valuable to obtain useful information regarding the nature of the lowest singlet excited states and it also can be used to estimate the value range and the relative ordering of energy gaps.

To investigate the effect of using different functionals for the DFT calculations of the electronic excitation energies of the charge-transfer-like molecules, one of the M06 families, M06-2X, has been used. M06-2X is newly emerged and has been proven to have similar accuracy to the well-known B3LYP [36]. As seen in Table 3, the HOMO and LUMO energy levels and the E_{H-L} and Eg values all exhibit great deviations. Deviations in the E_{H-L} values, in particular, may be due to the fact that the new functional contains a very large percentage of HF exchange.

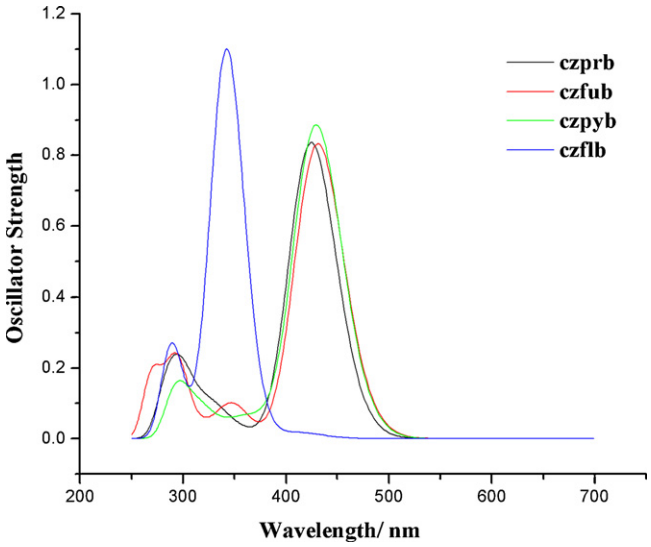

Fig. 5. Simulated emission spectra of title compounds in THF with the calculated data at the TDDFT/B3LYP/6-31G* level.

3.6. Absorption and emission spectra

To understand the electronic transitions of the fluorophores, TDDFT/B3LYP/6-31G* has been used based on optimized geometry, and only the molecules with singlet–singlet strong oscillators are reported. The solvent influence on the absorption and emission spectra of the title compounds in THF was simulated at the TDDFT/B3LYP/6-31G* level by the PCM model. The simulated emission spectra obtained by Gaussian functions with a half-width of 3000 cm^{-1} based on the 10 lowest singlet energies from the TDDFT/B3LYP/6-31(d) calculations in THF solvent are plotted in Fig. 5. The electron transition energies, the oscillator strengths and the primary compositions, both in the isolated gas phase and in THF solvent, are listed in Tables 4–6.

As shown in Table 4, and by the molecular orbitals in Fig. 3, all electronic transitions are of a π–π^* type, and excitation to the S_1 state nearly corresponds to the promotion of an electron from the HOMO to the LUMO in both the isolated gas phase and THF. All of the new fluorophores have absorption peaks comparable to those of czthb and great feasibility for modification by new cores, indicating their potential as optoelectronic molecules. When compared with other molecules in the isolated gas phase, the lowest lying singlet–singlet absorption wavelength of czprb with the strongest oscillator is blue-shifted, which is consistent with the changing trend in the HOMO/LUMO gaps described above. The oscillator strengths of the molecules in THF are larger than those in the isolated gas phase, indicating that a polar environment enhances the absorption strength of molecules with bipolar structures and is therefore beneficial to the fluorescent emission. The absorption wavelength in THF is red-shifted to some extent (average of 9.05 nm) due to the solvation effect that stabilizes the excited state. This shift can also be observed from the dipole moments of the first excited states in Table 2 probably because the electron density distribution of the LUMO can be stabilized by solvation, resulting in a decrease in the excited-state energy. A more polarized electron distribution in the excited state causes an increase in the solvent effect of THF. The czflb molecule shows quite different absorption spectra in THF because the more polarized electron distribution of the ground and excited states leads to increased solvent effects from THF. Table 4 shows that the strongest absorption

Table 4
Absorption spectra both in gas phase and THF solvent obtained by TDDFT methods and PCM model for title compounds at B3LYP/6-31G(d) optimized geometries.

		Excited state	Main composition		Excitation energies (eV)	λ (nm)	*f*
czprb	Gas phase	$s_0 \rightarrow s_1$	HOMO → LUMO	0.65	3.35	369.7	0.89
	THF	$s_0 \rightarrow s_2$	HOMO → LUMO	0.66	3.26	380.3	0.99
czfub	Gas phase	$s_0 \rightarrow s_1$	HOMO → LUMO	0.65	3.17	391	0.83
	THF	$s_0 \rightarrow s_2$	HOMO → LUMO	0.66	3.06	404.6	0.94
czpyb	Gas phase	$s_0 \rightarrow s_1$	HOMO → LUMO	0.67	3.14	394.3	0.68
	THF	$s_0 \rightarrow s_2$	HOMO → LUMO	0.68	3.06	404.7	0.77
czflb	Gas phase	$s_0 \rightarrow s_3$	HOMO-4 → LUMO	0.51	3.71	334.2	0.39
			HOMO-3 → LUMO	0.15			
			HOMO-2 → LUMO	−0.27			
			HOMO-1 → LUMO	−0.19			
			HOMO → LUMO + 1	−0.24			
		$s_0 \rightarrow s_1$	HOMO → LUMO	0.68	3.20	387.1	0.01
	THF	$s_0 \rightarrow s_3$	HOMO-4 → LUMO	−0.41	3.69	335.8	0.79
			HOMO-3 → LUMO	−0.13			
			HOMO-2 → LUMO	0.26			
			HOMO-1 → LUMO	0.21			
			HOMO → LUMO + 1	0.40			
		$s_0 \rightarrow s_1$	HOMO → LUMO	0.68	3.20	387.2	0.02

of czflb is the excitation from the ground state, S_0, to S_3, in both the gas phase and THF solvent. In addition, the oscillator strength of the $S_0 \rightarrow S_1$ transition is quite small indicating that the $S_0 \rightarrow S_1$ transition is forbidden. The strongest absorption wavelength of czflb is the shortest, and the configurations of the electronic excitation are rather dispersed potentially due to the nonplanar molecular structure of czflb. The main contribution to the electron transition does not arise from HOMO → LUMO but from the HOMO-4 → LUMO transition in both the gas phase and THF. It is interesting to note that the initial state of czflb is primarily related to the MO that localizes on the carbazole and fluorene moieties (Fig. 3), while its final state is primarily related to the MO that localizes on the dimesitylborane, indicating that the absorption transition is an intramolecular charge-transfer process. These particular MOs and their electron transition process may lead to the observed absorption behavior.

The theoretical emission calculations based on the optimized first singlet excited states under TDDFT/B3LYP/6-31G* level with the strongest oscillator are presented in Table 6. All chemical

Table 5
Absorption spectra both in gas phase and THF solvent obtained by TDDFT methods and SMD model for title compounds at M06-2X/6-31G(d) optimized geometries.

		Excited state	Main composition		Excitation energies (eV)	λ (nm)	*f*
czprb	Gas phase	$s_0 \rightarrow s_1$	HOMO-4 → LUMO	0.10	3.87	320.30	1.09
			HOMO-1 → LUMO	0.14			
			HOMO → LUMO	0.66			
	THF	$s_0 \rightarrow s_1$	HOMO-2 → LUMO	−0.16	3.79	326.90	1.22
			HOMO-1 → LUMO	0.16			
			HOMO → LUMO	0.64			
czfub	Gas phase	$s_0 \rightarrow s_1$	HOMO-3 → LUMO	−0.16	3.64	340.95	0.96
			HOMO-1 → LUMO	0.14			
			HOMO → LUMO	0.65			
	THF	$s_0 \rightarrow s_1$	HOMO-3 → LUMO	0.17	3.54	349.90	1.10
			HOMO-1 → LUMO	0.15			
			HOMO → LUMO	0.65			
czpyb	Gas phase	$s_0 \rightarrow s_1$	HOMO-6 → LUMO	0.11	3.83	323.90	0.96
			HOMO-3 → LUMO	−0.25			
			HOMO-2 → LUMO	0.14			
			HOMO-1 → LUMO	0.12			
			HOMO → LUMO	0.59			
			HOMO → LUMO + 2	−0.13			
	THF	$s_0 \rightarrow s_1$	HOMO-6 → LUMO	0.14	3.79	327.10	1.15
			HOMO-3 → LUMO	−0.22			
			HOMO-2 → LUMO	0.14			
			HOMO → LUMO	0.60			
			HOMO → LUMO + 2	−0.14			
czflb	Gas phase	$s_0 \rightarrow s_5$	HOMO-4 → LUMO	−0.21	4.44	278.90	1.13
			HOMO-2 → LUMO + 1	0.14			
			HOMO → LUMO + 1	0.59			
			HOMO → LUMO + 2	−0.16			
		$s_0 \rightarrow s_1$	HOMO-13 → LUMO	−0.14	4.10	302.30	0.10
			HOMO-3 → LUMO	0.67			
	THF	$s_0 \rightarrow s_4$	HOMO-4 → LUMO	0.35	4.32	287.10	1.29
			HOMO-2 → LUMO + 1	0.12			
			HOMO → LUMO	−0.26			
			HOMO → LUMO + 1	0.42			
			HOMO → LUMO + 2	−0.22			
		$s_0 \rightarrow s_1$	HOMO-13 → LUMO	−0.13	4.14	299.26	0.14
			HOMO-3 → LUMO	0.67			

Table 6
Emission spectra data obtained in both gas and solvent THF on the basis of TDDFT for the title compounds.

		Electron transition	Main composition		Excitation energies (eV)	λ (nm)	*f*	Radiative lifetimes (ns)
czprb	Gas phase	$s_1 \rightarrow s_0$	LUMO → HOMO	0.64	3.03	409.8	1.03	2.44
	THF	$s_1 \rightarrow s_0$	LUMO → HOMO	0.65	2.92	424.7	1.15	2.34
czfub	Gas phase	$s_1 \rightarrow s_0$	LUMO → HOMO	0.63	3.00	413.5	1.02	2.51
	THF	$s_1 \rightarrow s_0$	LUMO → HOMO	0.65	2.88	431.1	1.15	2.41
czpyb	Gas phase	$s_1 \rightarrow s_0$	LUMO → HOMO	0.64	3.02	411.1	1.09	2.32
	THF	$s_1 \rightarrow s_0$	LUMO → HOMO	0.66	2.89	429.5	1.22	2.26
czflb	Gas phase	$s_5 \rightarrow s_0$	LUMO → HOMO-6	0.18	3.74	331.7	0.50	3.29
			LUMO → HOMO-5	0.15				
			LUMO → HOMO-4	0.12				
			LUMO → HOMO-1	0.47				
			LUMO + 1 → HOMO	−0.41				
	THF	$s_3 \rightarrow s_0$	LUMO → HOMO-4	0.36	3.57	347.7	0.79	2.29
			LUMO → HOMO-3	0.13				
			LUMO → HOMO-2	−0.32				
			LUMO → HOMO-1	−0.30				
			LUMO + 1 → HOMO	−0.34				

modifications of the known fluorophores (czthb and czphb) result in materials with blue-shifted light-emitting features. By comparing the calculated results with the relevant values for these compounds in the gas phase (Table 6), the emission spectra in THF solvent have been found to be red-shifted (15–19 nm), but their oscillator strengths have increased due to the fact that the solvent stabilizes their excited states, These changes in emission spectra and oscillator strength are coincident with the changes observed in the absorption spectra. The calculated emission spectra of each compound are also found to be nearly the same in their respective phases. The emission spectra with the strongest oscillators arising from the S_1 states with $\pi^* \rightarrow \pi$ and LUMO → HOMO transition character (Fig. 3) for the first three materials. These transitions are coincident with those observed in the absorption spectra. While the emission spectra with strongest oscillator for czflb arises from the S_5 state in the gas phase and from the S_3 state in THF with a complex transition composition. The differing initial points of emission may be due to the positive solvent effect for the excited-state geometry. As shown in Fig. 5 and Table 6, the calculated values of the fluorescent wavelengths for these compounds in THF are located at 424.7 nm, 431.1 nm, 429.5 nm, and 347.7 nm. As with the observed energy gaps, the emission wavelengths of czfub and czprb exhibit a blue-shift when compared with those of czthb, while the emission wavelength of czpyb exhibits a slight red-shift. These observations are primarily due to the electron-donation ability of the core moieties. A stronger electron-donation ability of the core leads to larger energy gaps, and with the larger energy gaps, the emission wavelengths and absorption wavelengths are blue-shifted. These results are in accordance with the required wavelengths for blue or deep-blue materials when compared with the spectral data of czthb. When the optical values in Table 4 are compared with those in Table 6, the Stokes shifts of these compounds are found to be in the range of 16.8–40.1 nm in the gas phase and in the range of 11.9–44.4 nm in THF, suggesting a greater rearrangement of the fluorophores upon photoexcitation. As with the above observations, the pyrrol ring in czprb is nonplanar in the ground state, but it becomes more planar when shifted to the first singlet excited state.

The radiative lifetimes (in au) have been computed for spontaneous emission using the Einstein transition probabilities according to the following formula [37]:

$$\tau = \frac{c^3}{2(E_{\mathrm{Flu}})^2 f}$$

where c is the velocity of light, E_{Flu} is the excitation energy, and f is the oscillator strength. The computed lifetimes, τ, for the title compounds both in the gas phase and in THF are listed in Table 6. Short radiative lifetimes lead to high light-emitting efficiency, while long radiative lifetimes facilitate electron and energy transfer. In THF, the radiative lifetimes of compounds are shorter with increased oscillator strength, leading to an increase in the luminescent efficiency in solution.

For a comparison of different functional effects and different solvation model effects, M06-2X has been carried out, and the influence of the solvent (THF) on the absorption spectra has been simulated using an SMD model. The influence of the different solvation models for czprb and czfub has been listed in Table S3. Table S3 shows that the effects of the different solvation models on the absorption spectra are nearly the same. Following the comparison of the absorption spectra in the gas phase as computed by B3LYP and M06-2X (Tables 4 and 5), the new computing method was found to lead to great blue-shifting and dispersive electronic transitions. The M06-2X method reveals deep-seated electronic transitions such as HOMO-4 → LUMO in both the gas phase and THF.

3.7. Ionization potentials and electron affinities

Because the performance of OLED devices primarily depends on the charge injection, transfer, balance, and the exciton confinement in the light-emitting layer, an adequate and balanced transporting of both the injected electron and hole is crucial to improving the performance of OLED devices. The IPs and EAs are well-defined properties that can be calculated by DFT to estimate the energy barriers for the injections of both hole and electron into the molecules. Table 7 contains the IPs and EAs both vertical (v, at the geometry of the neutral molecule) and adiabatic (a, at the optimized structure for both the neutral and charged molecule), and the extraction potentials (HEP and EEP for the hole and electron, respectively) that refer to the geometry of the ions [38]. HEP is the energy difference from M (neutral molecule) to M^+ (cation), using the M^+ geometric structure in the calculation, and EEP is the energy difference from M to M^- (anion), using the M^- geometric structure in the calculation.

Presently, two types of models have been used to evaluate the charge (hole and electron) mobility [39]. One model is the coherent band model [40], and the other is the incoherent hopping model [41]. The latter is suitable for most organic molecular materials [42] in which the coupling between neighboring molecules is small, and is thus chosen for our study. In the second model, the charge transport is an intermolecular process in which the charge hops between two adjacent molecules. This process can be summarized as follows:

$$M^{+/-} + M \rightarrow M^{+}M^{+/-}$$

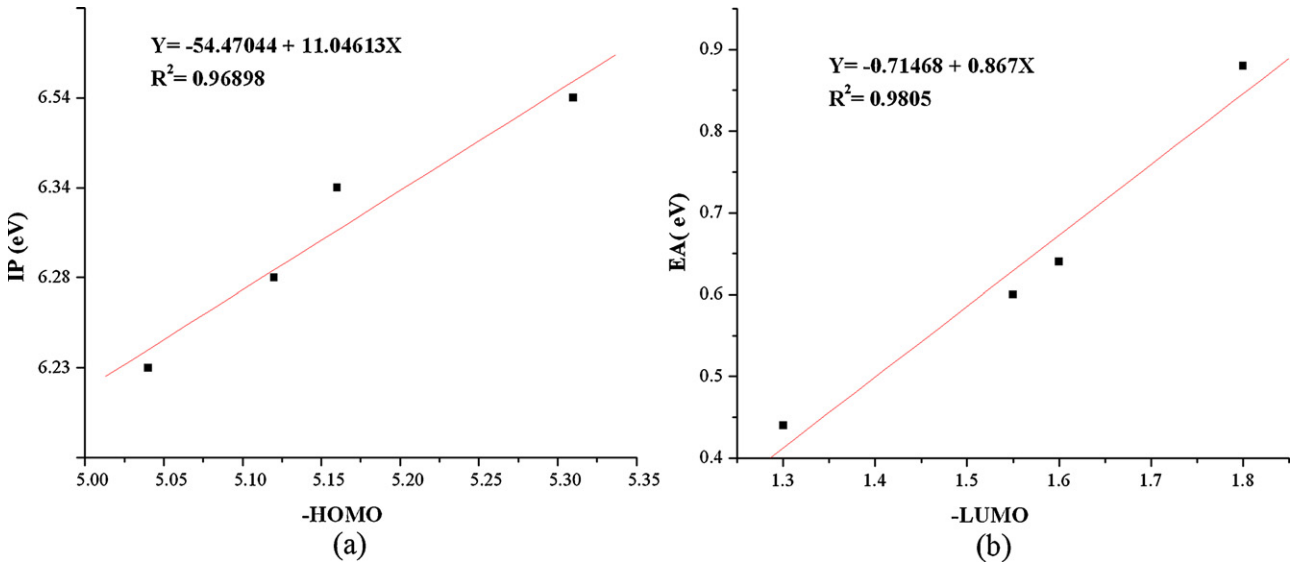

Fig. 6. (a) The correlation between the calculated HOMO energies and the IP values. (b) The correlation between the calculated LUMO energies and the EA values.

Table 7
IPs, EAs and extraction potentials for each molecule (eV).

	IP(v)	IP(a)	HEP	EA(v)	EA(a)	EEP
czprb	6.23	6.05	5.85	0.44	0.31	0.16
czfub	6.34	6.23	6.08	0.64	0.54	0.44
czpyb	6.54	6.44	6.38	0.88	0.76	0.64
czflb	6.28	6.15	6.02	0.60	0.49	0.39

where M is the neutral molecule interacting with neighboring oxidized or reduced $M^{+/-}$.

One challenge in the application of small molecule OLEDs is the achievement of high EA for improving the electron injection/transport and the achievement of low IP for improving hole injection/transport. In luminescent materials, a lower IP of the hole-transporting layer (HTL) leads to an easier entrance of a hole from the anode to the HTL. In addition, a higher EA value for the electron-transport layer (ETL) leads to an easier entrance of electrons from the cathode to the ETL. As shown in Table 7, the energies required to create a hole in czfub, czprb, czpyb, and czflb are 6.05, 6.34, 6.54, and 6.28 eV, respectively, and the energies required to accept an electron in these compounds are 0.44, 0.64, 0.88, and 0.60 eV, respectively. The ability to create holes decreases, and the trends in the IPs and EAs for these compounds are similar to the trends in the negative values of their HOMO and LUMO levels. The linear correlations between the IP and EA values and the relevant negative values of the HOMO and LUMO energy levels can be obtained according to the following equations (Fig. 6):

$$\mathrm{IP} = -54.47044 + 11.04613(-E_{\mathrm{HOMO}}) \quad R^2 = 0.96898$$

$$\mathrm{EA} = -0.71468 + 0.867(-E_{\mathrm{LUMO}}) \quad R^2 = 0.9805$$

where R^2 is the regression constant. Although the IP and EA values of other carbazole-π-dimesitylborane bipolar fluorophores are still unknown, these regression equations could provide a simple formula to predict the IPs and EAs of other fluorophores from their frontier molecular orbital energies. This calculation also confirms the findings regarding the HOMO and LUMO energies and provides an in-depth interpretation of the electronic properties of these compounds.

Experiments have proven that Mes_2B [*p*-4,4′-biphenyl-NPh(1-naphthyl)] (BNPB) is a good trifunctional molecule [43]. Its IP and EA values are 6.08 eV and 0.77 eV, respectively. Thus, in comparing the relevant values of the title compounds with those of BNPB, the electron injection/transport property of czpyb is found to be best. Furthermore, when compared with czthb (Fig. S1), the pyrrol-based compound is observed to be a better hole-transporting material, and the pyridine-based compound could be a better electron accepter.

4. Conclusion

In summary, a series of arylborane-containing carbazole bipolar fluorophores have emerged for the potential fabrication of highly efficient nondoped blue OLEDs, and theoretical investigations based on quantum chemical calculations of their structural and electronic properties have been carried out. The following conclusions can therefore be drawn: (1) The calculated results show that the optical and electronic properties (HOMOs, LUMOs, energy gaps, absorption and emission spectra, IPs, EAs and radiative lifetimes) of the potential fluorophore materials are all affected by differing π conjugations. (2) The compounds, czfub and czpyb, exhibit good planar configurations and better optoelectronic qualities than the experimental compounds. Additionally, the IP and EA values show czpyb and czprb to be the best electron-transporting and hole-transporting materials, respectively. (3) In comparison with the calculated results of the newly emerged compounds in the gas phase, the absorption and emission spectra with increasing oscillator strength are red-shifted in the THF solvent phase, and the emission wavelengths in THF of all of the compounds are located in the blue to deep-blue range. (4) The czflb compound exhibits similar optoelectronic properties to those of czfub, indicating that a larger-sized fluorene core does not have a positive effect on the electronic structure of entire molecule. The DFT results provide insight into the nature of bipolar molecules and show that the new fluorophores could meet the requirements of a host material for blue emissions.

Acknowledgments

This work is supported by the Training Fund of NENU'S Scientific Innovation Project (NENU-STC07016). We are sincerely thankful for the reviewers' helpful comments.

Appendix A. Supplementary data

Supplementary data associated with this article can be found, in the online version, at doi:10.1016/j.jmgm.2011.12.007.

References

[1] C.W. Tang, A.S. Van slyke, Organic electroluminescent diodes, Appl. Phys. Lett. 51 (1987) 913–915.
[2] M.A. Baldo, M.E. Thompson, S.R. Forrest, High-efficiency fluorescent organic light-emitting devices using a phosphorescent sensitizer, Nature 403 (2000) 750–753.
[3] Y.R. Sun, N.C. Giebink, H. Kanno, B.W. Ma, M.E. Thompson, S.R. Forrest, Management of singlet and triplet excitons for efficient white organic light-emitting devices, Nature 440 (2006) 908–912.
[4] C.G. Zhen, Z.K. Chen, Q.D. Liu, Y.F. Dai, R.Y.C. Shin, S.Y. Chang, J. Kieffer, Achieving highly efficient fluorescent blue organic light-emitting diodes through optimizing molecular structures and device configuration, J. Adv. Mater. 21 (2009) 699–707.
[5] D. Vak, B. Lim, S.H. Lee, D.Y. Kim, Synthesis of a double spiro-polyindenofluorene with a stable blue emission, Org. Lett. 7 (2005) 4229–4232.
[6] A.P. Kulkarni, S.A. Jenekhe, Blue light-emitting diodes with good spectral stability based on blends of poly(9,9-dioctylfluorene): interplay between morphology, photophysics, and device performance, Macromolecules 36 (2003) 5285–5296.
[7] R.C. Chiechi, R.J. Tseng, F. Marchioni, Y. Yang, F. Wudl, Efficient blue-light-emitting electroluminescent devices with a robust fluorophore: 7,8,10-triphenylfluoranthene, Adv. Mater. 18 (2006) 325–328.
[8] L.M. Leung, W.Y. Lo, S.K. So, K.M. Lee, W.K. Choi, A high-efficiency blue emitter for small molecule-based organic light-emitting diode, J. AM. Chem. Soc. 122 (2000) 5640–5641.
[9] M.T. Lee, C.H. Liao, C.H. Tasi, C.H. Chen, Highly efficient, deep-blue doped organic light-emitting devices, Adv. Mater. 17 (2005) 205–211.
[10] C.C. Wu, Y.T. Lin, K.T. Wong, R.T. Chen, Y.Y. Chen, Efficient organic blue-light-emitting devices with double confinement on terfluorenes with ambipolar carrier transport properties, Adv. Mater. 16 (2004) 61–65.
[11] C.W. Tang, S.A. Van slyke, C.H. Chen, Electroluminescence of doped organic thin films, J. Appl. Phys. 65 (1989) 3610–3616.
[12] W.-C. Wu, H.-C. Yeh, L.-H. Chan, C.-T. Chen, Red organic light-emitting diodes with a non-doping amorphous red emitter, Adv. Mater. 14 (2002) 1072–1075.
[13] C.-T. Chen, Evolution of red organic light-emitting diodes: materials and devices, Chem. Mater. 16 (2004) 4389–4400.
[14] S.L. Lin, L.H. Chan, R.H. Lee, M.Y. Yen, W.J. Kuo, C.T. Chen, R.J. Jeng, Highly EFfiCIENT CARBAZOLE-p-dimesitylborane bipolar fluorophores for nondoped blue organic light-emitting diodes, Adv. Mater. 20 (2008) 3947–3952.
[15] Z.W. Liu, M. Guan, Z.Q. Bian, D.B. Nie, Z.L. Gong, Z.B. Li, C.H. Huang, Red phosphorescent iridium complex containing carbazole-functionalized β-diketonate for highly efficient nondoped organic light-emitting diodes, Adv. Funct. Mater. 16 (2006) 1441–1448.
[16] Y. Shirota, M. Kinoshita, T. Noda, K. Okumoto, T. Ohara, A novel class of emitting amorphous molecular materials as bipolar radical formants: 2-{4-[Bis(4-methylphenyl)amino]phenyl}-5-(dimesitylboryl)thiophene and 2-{4-[Bis(9,9-dimethylfluorenyl)amino]phenyl}-5-(dimesitylboryl)thiophene, J. Am. Chem. Soc. 122 (2000) 11021–11022.
[17] T.-H. Huang, J.T. Lin, L.-Y. Chen, Y.-T. Lin, C.-C. Wu, Dipolar dibenzothiophene *SS*-dioxide derivatives containing diarylamine: materials for single-layer organic light-emitting devices, Adv. Mater. 18 (2006) 602–606.
[18] H. Doi, M. Kinoshita, K. Okumoto, Y. Shirota, A novel class of emitting amorphous molecular materials with bipolar character for electroluminescence, Chem. Mater. 15 (2003) 1080–1089.
[19] K. Panthi, R.M. Adhikari, T.H. Kinstle, Carbazole donor-carbazole linker-based compounds: preparation, photophysical properties, and formation of fluorescent nanoparticles, J. Phys. Chem. A 114 (2010) 4550–4557.
[20] G.S. Jiao, L.H. Thoresen, K. Burgess, Through-bond energy transfer cassettes for labeling multiple biological molecules in one experiment, J. Am. Chem. Soc. 125 (2003) 14668–14669.
[21] M.S. Wong, Z.H. Li, Y. Tao, M. D'Iorio, Synthesis, Functional properties of donor–acceptor π conjugated oligomers, Chem. Mater. 15 (2003) 1198–1203.
[22] M.A. Loi, P. Denk, H. Hoppe, H. Neugebauer, C. Winder, D. Meissner, C. Brabec, N.S. Sariciftci, A. Gouloumis, P. Vazquezb, T.J. Torresb, Mater. Chem. 13 (2003) 700–704.
[23] X.H. Ouyang, H.P. Zeng, Theoretical predication on optical and electronic properties of multifunctional molecules for blue-light multifunctional materials, Theochem 945 (2010) 71–77.
[24] M.J. Frisch, et al. Gaussian 03, Revision C.02, Gaussian Inc., Pittsburgh, PA, 2003.
[25] A.D. Becke, A newmixing of Hartree–Fock and local density-functional theories, J. Chem. Phys. 98 (1993) 1372–1377.
[26] C. Lee, W. Yang, R.C. Parr, Development of the Colle–Salvetti correlation-energy formula into a functional of the electron density, Phys. Rev. B 37 (1998) 785–789.
[27] Y. Zhao, D.G. Truhlar, Density functionals with broad applicability in chemistry, Acc. Chem. Res. 41 (2008) 157–167.
[28] Y. Zhao, D.G. Truhlar, A new local density functional for main-group thermochemistry transition metal bonding, thermochemical kinetics, and noncovalent interactions, J. Chem. Phys. 125 (2006) 194101–194108.
[29] Y. Zhao, D.G. Truhlar, Density functional for spectroscopy: no long-range self-interaction error, good performance for rydberg and charge-transfer states, and better performance on average than B3LYP for ground states, J. Pys. Chem. A 110 (2006) 13126–13130.
[30] N.E. Schultz, Y. Zhao, D.G. Truhlar, Density functionals for inorganometallic and organometallic chemistry, J. Pys. Chem. A 109 (2005) 11127–11143.
[31] J. Morin, M. Leclerc, D. Ades, A. Siove, Polycarbazoles: 25 years of progress, Macromol. Rapid Commun. 26 (2005) 761–778.
[32] M.A. De Oliveira, H.A. Duarte, J.M. Pernaut, W.B. De Almeida, Energy gaps of α,α'-substituted oligothiophenes from semiempirical, *ab initio*, and density functional methods, J. Phys. Chem. A 104 (2000) 8256–8262.
[33] W.Y. Wong, Z. He, S.K. So, K.L. Tong, Z. Lin, A multifunctional platinum-based triplet emitter for OLED applications, Organometallics 24 (2005) 4079–4082.
[34] P.J. Hay, Theoretical studies of the ground and excited electronic states in cyclometalated phenylpyridine Ir(III) complexes using density functional theory, J. Phys. Chem. A 106 (2002) 1634–1641.
[35] C.J. Tonzola, A.P. Kulkarni, A.P. Gifford, W. Kaminsky, S.A. Jenekhe, Blue-light-emitting oligoquinolines: synthesis properties and high-efficiency blue-light-emitting diodes, Adv. Funct. Mater. 17 (2007) 863–874.
[36] D. Jacquemin, E.A. Perpète, H. Ciofini, C. Adamo, R. Valero, Y. Zhao, D.G. Truhlar, Assessment of functionals for TD-DFT calculations of singlet triplet transitions, JCTC 6 (2010) 2071–2085.
[37] V. Lukěs, A. Aquino, H. Lischka, Theoretical study of vibrational and optical spectra of methylene-bridged oligofluorenes, J. Phys. Chem. A 109 (2005) 10232–10238.
[38] A. Curioni, M. Boero, W. Andreoni, A Alq_3: ab initio calculations of its structural and electronic properties in neutral and charged states, Chem. Phys. Lett. 294 (1998) 263–271.
[39] B. Yang, S.K. Kim, H. Xu, Y.I. Park, H.Y. Zhang, C. Gu, F.Z. Shen, C.L. Wang, D.D. Liu, X.D. Liu, M. Hanif, S. Tang, W.J. Li, F. Li, J.C. Shen, J.W. Park, Y.G. Ma, The origin of the improved efficiency and stability of triphenylamine-substituted anthracene derivatives for OLEDs: a theoretical investigation, Chem. Phys. Chem. 9 (2008) 2601–2610.
[40] Y. Yang, H. Geng, S.W. Yin, Z.G. Shuai, J.B. Peng, First-principle band structure calculations of tris(8-hydroxyquinolinato)aluminum, J. Phys. Chem. B 110 (2006) 3180–3184.
[41] B.C. Lin, C.P. Cheng, Z.Q. You, C.P. Hsu, Charge transport properties of tris(8-hydroxyquinolinato)aluminum(III): why It Is an Electron Transporter J, Am. Chem. Soc. 127 (2005) 66–67.
[42] J. Yin, R.F. Chen, S.L. Zhang, Q.D. Ling, W. Huang, Theoretical studies of the structural, electronic, and optical properties of phosphafluorenes, J. Phys. Chem. A 114 (2010) 3655–3667.
[43] W.L. Jia, X.D. Feng, D.R. Bai, Z.H. Lu, S.G. Wang, Vamvounis, Mes_2B(*p*-4 4'-biphenyl-NPh(1-naphthyl)). A multifunctional molecule for electroluminescent devices, Chem. Mater. 17 (2005) 164–170.